Hindawi
Advances in Civil Engineering
Volume 2024, Article ID 6305640, 14 pages
https://doi.org/10.1155/2024/6305640

Research Article

Research on Hydraulic Fracturing Technology of Long Boreholes along Strata of High Vast Thick Coal Seam

Chenyang Wang,[1,2] **Shugang Li**,[1] **Li Liu**,[1] **and Le Liu**[2]

[1]*Safety College, Xi'an University of Science and Technology, Xi'an 710054, China*
[2]*Xi'an Research Institute (Group) Co. Ltd., China Coal Technology and Engineering Group Corp., Xi'an 710077, China*

Correspondence should be addressed to Chenyang Wang; wangchenyang@cctegxian.com and Le Liu; leliu1208@yeah.net

Received 26 September 2023; Revised 25 November 2023; Accepted 27 January 2024; Published 6 March 2024

Academic Editor: Tingting Zhang

Gas extraction is a major technique for regional gas regulation and coal and gas comining in China. Assuring effective gas extraction operations is a crucial step in ensuring the supply of energy. The effect range of extraction drilling, pressure relief degree, and standard period of gas extraction are all constrained because of the geological constraints affecting coal gas permeability and occurrence. Combined with the advantages of directional drilling and high-efficiency pumping technology and antireflection enhanced pumping technology of hydraulic fracturing, directional long-drilling hydraulic fracturing can effectively improve the efficiency of gas control and expand the scale of gas control. The present study focuses on the exploration of directional long-hole hydraulic fracturing technique in thick coal seams with high gas content using Dafosi Mine as a case study. The research findings demonstrate that hydraulic fracturing contributes to the enlargement of pore size, pore density, and pore connectivity in coal seams. In-depth research was conducted on the expansion of coal seam fractures during the hydraulic fracturing process using the RFPA3D-flow numerical simulation program. Additionally, a comprehensive analysis of stress distribution around the fractures under the flow-solid coupling condition was performed. To further improve the effectiveness of hydraulic fracturing technique, the research team optimized the fracturing tools and construction processes in the four coal seams of Dafosi Mine. The impact of segmented hydraulic fracturing in coal seam bare hole drilling was also studied. Furthermore, an investigation method specific to the coal seam bare hole segmented hydraulic fracturing effects applicable to Dafosi Mine was developed. The maximum fracture extension pressure, minimum fracture closure pressure, and fracture morphology change characteristics during drilling and fracturing were measured, and the fracturing influence radius of coal seam was determined to be 46−58 m, the gas extraction concentration after fracturing increased by 2.20–4.22 times, and the 100-m extraction flow increased by 4.93–11.03 times. It gives other mines technical assistance so they can keep advocating and utilizing the horizontal directional long-drilling stage hydraulic fracturing technique.

1. Introduction

To manage regional gas levels and sustain China's comining of coal and gas, gas extraction is crucial [1–3]. It has several advantages, including reducing gas emissions during mining, preventing gas from building up and beyond safe limits, preventing gas explosions, and putting an end to coal and gas outburst accidents. Furthermore, it can convert waste into a protective resource and make use of gas as a valuable coal-related resource [4–7]. The progress made by China in gas extraction technology has many benefits, including environmental protection, efficient resource utilization, and safe production. Additionally, this technology can improve energy effectiveness and guarantee the safety of mines and miners [8–11]. Many coal seams in China have limited permeability, which has a negative impact on direct gas extraction efficiency and raises production costs. To raise the permeability of coal seams and increase the effectiveness of gas extraction, artificial approaches must be used [12–16]. Hydraulic fracturing is a technology for extracting gas. It involves injecting high-pressure water or liquid into coal seam rock to cause it to fracture and expand, thereby increasing the efficiency of gas release and collection [17–20].

Considerable research has been carried out by experts and scholars worldwide on the utilization of hydraulic

fracturing methods for increasing gas extraction efficiency in underground mining. Wang et al. [21], following an investigation into the detrimental effects of high-pressure water jets on coal and the technology of inducing stress relief and permeability enhancement through hydraulic flushing cavities, introduced the concept of floor rock roadways equipped with hydraulic flushing cavities. Based on the numerical simulation results, modifying the cavity structure can effectively alleviate stress concentration between cavities, thereby allowing for extensive stress relief and permeability enhancement. Song et al. [22] performed numerical simulation experiments to assess the impact of natural fractures on hydraulic fracture propagation. They investigated the effects of various factors, including the approaching angle, differential principal stress, length and strength of natural fractures, reservoir elastic modulus, and Poisson's ratio. Furthermore, they conducted a semi-analytical exploration and optimization of stress-related permeability models for coalbed methane (CBM) reservoirs. Nainar and Govindarajan [23] created a novel pressure-dependent model that is adaptable to variations in reservoir temperature and adsorption strain. Wang et al. [21] conducted a study on the technology to reduce reflections in high-pressure water jet drilling for expanding coal seams. Their objective was to address the challenges posed by severe outbursts and gas emissions in hazardous coal seams under complex geological conditions. To achieve this, they employed an integrated water jet drilling and expansion device and implemented high-pressure expansion measures at the working face, aiming to improve the efficiency of coal seam gas extraction. Mou et al. [24] conducted a study on the influence of hydraulic fracturing on high-rank coal microfractures under different stress conditions. The researchers noted that stronger heterogeneity and larger differences in horizontal stress would hinder the expansion of microfractures. Conversely, smaller differences in horizontal stress would promote more uniform expansion of microfractures during hydraulic fracturing, thereby facilitating their connectivity. Lu et al. [25] conducted a comprehensive exploration of the dynamic variations in coal fracture and pore structure during the hydraulic fracturing process. Their findings are of paramount significance for precise permeability prediction, successful advancement of hydraulic fracturing technology, and improved productivity of CBM. Thus, it is vital to prioritize and leverage their research achievements to foster industry development.

To increase CBM's permeability and increase extraction effectiveness under geophysical circumstances such as coal seam fluctuation and ground stress, these researchers conducted in-depth research on hydraulic fracturing. The traditional hydraulic fracturing approach has a restricted impact area on drainage boreholes, leading to inadequate pressure release, and prolonged attainment of gas extraction compliance. Such limitations unfavorably affect the sequential operations of mining, extraction, and excavation. This article recommends the use of directional long-drilling hydraulic fracturing to shatter high gas thick coal seams. To widen the fracture and connect the coal seam, this technique entails drilling into the target layer below the earth and injecting high-pressure liquid. As a result, the coal seam's gas permeability and release rise. Directional long-drilling hydraulic fracturing is more accurate and controllable than conventional hydraulic fracturing, enabling the extraction of gas from certain areas and coal seams. Applying this method can efficiently improve gas treatment efficiency, expand the scale of gas treatment, and achieve higher gas recovery benefits.

2. Overview of Mine and Work Expand

The Dafosi Mine is a modern and large mine developed and constructed by Binchang Company. It is situated about 160 km from Xi'an at the southern boundary of the Binchang Mining region, near the intersection of Binzhou City and Changwu County. There are uncommon and basic structural faults in the mining area. The Xiagou Coal Mine, Shuilandong Coal Mine, Jiangjiahe Coal Mine, Yangjiaping Mine Field, Tingnan Coal Mine, and Xiaozhuang Coal Mine are all close by to the east, south, west, north, and northeast, respectively, of the Dafosi Mine. Figure 1 shows the traffic flow diagram for the coal mine. With an absolute emission of 160.69 m^3/min and a relative emission of 12.93 m^3/t, the mine emits a lot of gas. The coal seam gas characteristics were measured during the production process, and 4# coal had a gas content ranging from 3.5 to 5.9 m^3/t. The gas permeability coefficient is 0.25 m^2/MPa^2.

The working face located in Figure 2 has a strike length of 1,918 m and a dip length of 200 m. The coal seam's floor elevation ranges between 610 and 680 m. With higher elevations in the east and north and lower elevations in the west and south, the seam often runs approximately east–west and north–south. The coal seam has an average underground depth of 408 m and a maximum depth of 483 m. The coal seam has an average thickness of 15 m and is considered stable and extra thick. The structure of the seam is simple, with some containing 0–2 layers of dirt, mostly composed of carbonaceous mudstone. The coal seam has an average dip angle between 3° and 11° and is thickest in the east and thinnest in the west. Each channel's absolute gas output during the mining process ranges from 8 to 12 m^3/min, for a total gas emission of 74.25 m^3/min.

3. Feasibility of Hydraulic Fracturing of Coal Seam

High-pressure water can cause cracks, voids, and cavities to form within the coal seam. This results in the movement of the coal mass and enlargement of existing fissures, thereby increasing the porosity of the coal in the fractured boreholes. Consequently, this alters the permeability and pore structure characteristics of the coal, ultimately enhancing gas extraction efficiency [26–31]. Simulated experiments were run on coal samples to see how hydraulic fracturing altered their pore structure to study these alterations [32–36]. Scanning electron microscopy was used to compare and analyze the characteristics of coal pore structure before and after fracturing under different magnifications.

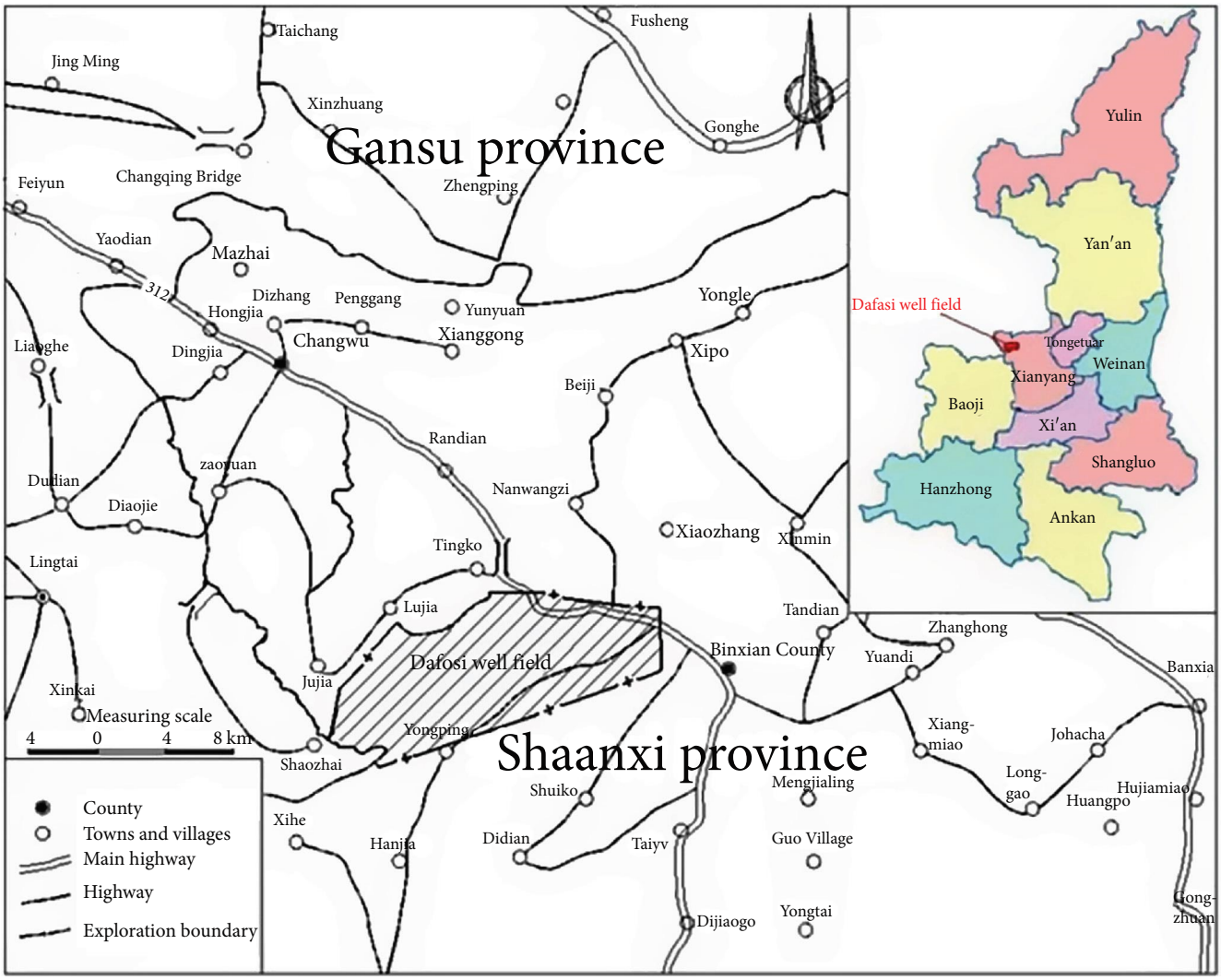

Figure 1: Schematic diagram of traffic location.

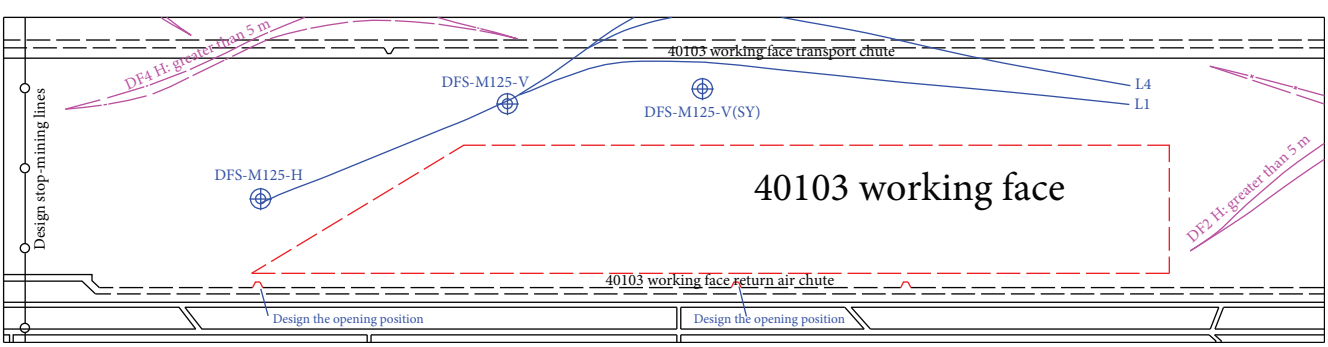

Figure 2: Location of 40103 working face.

3.1. Hydraulic Fracturing Experiment Test

3.1.1. Coal Sample Hydraulic Fracturing Test. Coal samples for testing were provided from the 4# coal seam of the Dafosi Coal Mine in Binchang District, Shaanxi Province. Prior to conducting the tests, larger coal samples are fragmented into smaller chunks to accommodate the volume of the cylindrical container. The smaller coal fragments were then placed into the fracturing cylinder, and the cylinder cover was secured. The valve was opened to allow for water injection and pressure monitoring when the pipeline was connected. The pressure gauge was used to observe any changes in water

Figure 3: Indoor fracturing equipment.

Figure 4: JSM-6460LV high-resolution electron microscope.

pressure. Once the water pressure reached the desired level of 15 MPa, the valve was closed to stop water injection, and the pressure was maintained for 48 hr. The indoor hydraulic fracturing machinery utilized in the procedure is shown in Figure 3.

Figure 4 shows the micromorphology traits that were discovered using a high-resolution electron microscope, the JSM-6460LV. Using conductive adhesive, the test coal sample is firmly fixed to the sample table after which the surface is painstakingly cleaned with a washing ear ball. A conductive material (gold) is then sprayed onto the sample surface. The acceleration voltage, probe diameter, probe current, and magnification are all adjusted based on the working distance and angle of the sample. Finally, by imaging the top observation plane of the coal sample, the surface morphology of the observation section is acquired at various magnifications.

3.1.2. Test Results of Coal Seam Hydraulic Fracturing. The test results showed that when exposed to high-pressure water, the coal sample broke into two smaller pieces. Figure 5 shows the sample's appearance both before and after fracture.

The coal sample was further crushed and sorted using a 200-mesh sieve with a 200-mesh diameter before being scanned with an electron microscope. The sample was then dried at 105°C before being tested. Figure 6 shows high-resolution electron microscope images of the sample both before and after fracturing.

Due to bedding, fracture fissures, and primary microfissures, coal contains numerous dense pores and fissures that are dispersed throughout its mass. There are three different varieties of these pores and fissures: those that are mutually connected, partially connected, and not connected [37–40]. Figure 6 demonstrates that following fracturing, the pores in coal samples grow and pore connection is strengthened. Hydraulic fracturing can increase the porosity and permeability of tight coal by enlarging the pores and fissures, making the extraction of coal seam gas more effective.

Using high-pressure water and hydraulic fracturing, weak areas within a coal seam are opened, expanded, and lengthened [41, 42]. By dividing the coal seam's structure, the action also increases the spatial volume of the cracks and creates a network of interlocking multicrack connectivity [43, 44]. The coal seam's permeability is significantly improved as a result. Coal samples had more holes and fractures, higher pore sizes, and a much better connection between pores and fractures after hydraulic fracturing. The microstructure and pore properties of coal have been improved because of the hydraulic fracturing of the Dafosi coal seam.

3.2. Numerical Simulation of Hydraulic Fracturing. Based on the geological parameters of the mining area, hydraulic fracturing during the drilling process was modeled using RFPA software. A 2D plane stress model was employed to generate a model with a longitudinal length of 200 m, transverse width of 120 m, and vertical height of 100 m. The complete model was partitioned into 2.4 million individual elements, measuring $200 \times 120 \times 100$ in size. The model configuration is depicted in Figure 7.

The mechanical parameters of coal seam adopted by the model are shown in Table 1.

In this simulation, a uniformity coefficient is used to evaluate the physical property uniformity in coal and rock materials. The actual mechanical properties of coal and rock materials are connected to uniformity, and these values are used to input the micromechanical parameter values for the numerical simulation [45–47]. The Weibull distribution is used to assign properties to the coal and rock materials, while the damage constitutive relationship is based on the Mohr–Coulomb criterion [48, 49].

We can determine the characteristics of fissure expansion that take place throughout the ensuing fracturing process by analyzing the various stages shown in Figure 8.

Step 1: The excavation process is initiated by the model, and boundary loads are applied resulting in the borehole filling up with water.

Step 55: The coal seams on either side of the drilling and fracturing section started to break and expand at an injection pressure of 8 MPa. More fractures were present

(a) (b)

Figure 5: Comparison of coal samples before and after fracturing: (a) coal sample before fracturing and (b) coal sample after fracturing.

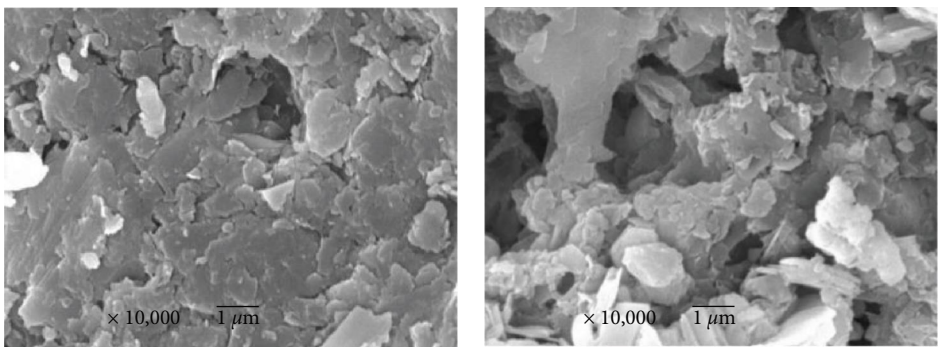

(a) (b)

Figure 6: Comparison of surface structures of coal samples before and after fracturing: (a) coal sample before fracturing and (b) coal sample after fracturing.

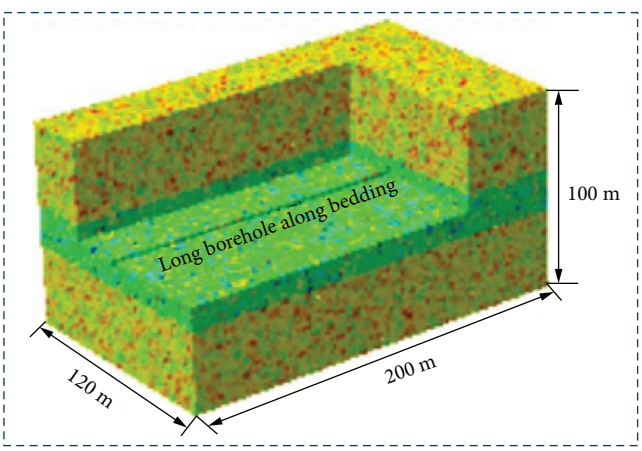

Figure 7: Numerical model of hydraulic fracturing.

on the left side than on the right, and as they spread out in a fan-like pattern, numerous microfracture networks were created.

Step 58: The crack kept growing and a network of microfractures was formed at a water injection pressure of 8.6 MPa. There are two ways to categorize the direction of the fracture extension: perpendicular to the drilling direction, with the left crack expanding by about 10 m and the right crack by about 13 m; and parallel to the drilling direction, with an expansion range of roughly 16.5 m.

Step 63: As the fractured rock undergoes further expansion, it forms three primary fissures. The first one is located parallel to and on the left side of the borehole. The second one connects the left and right sides of the borehole by a vertical fissure and intersects it perpendicularly. In relation to the borehole, the third fissure is positioned at an angle. Numerous microcracks that help to create a more complex microfracture network can be found close to these three primary cracks.

Step 65: The fracture continues to expand in the original direction when the water pressure that was injected approaches 10.0 MPa, leading to a significant increase in the length and width of the fracture. The major fracture is roughly 50 m long on both sides of the drilling, whereas the fracture that runs perpendicular to the drilling path is around 46 m long.

Step 68: The crack widened in the direction of the maximum primary stress as the water injection pressure reached 10.6 MPa. In addition to being noticeably wider, the fracture on the drilling hole's left side had a range that was noticeably greater than the one on the right. The crack spanned ∼58 m vertically and 75 m horizontally.

Figure 9 shows the cloud map of pore water pressure during hydraulic fracturing. According to Step 1, when water

Table 1: Mechanical parameters of coal seam adopted by the model.

Type	Coal seam	Type	Coal seam
Degree of uniformity	6	Permeability coefficient (md)	0.1
Elastic modulus (MPa)	1,298	Void pressure coefficient	0.4
Poisson's ratio, μ	0.23	Compressive strength (MPa)	6.5
Friction angle (degree)	28	Coupling coefficient	0.3
Pressed rabi	10	Bulk weight (kg/m^3)	1,390
Initial porosity of coal seam (%)	5.84	Adsorption constant, a (MPa^{-1})	29.70
Adsorption constant, b (MPa^{-1})	0.184	—	—

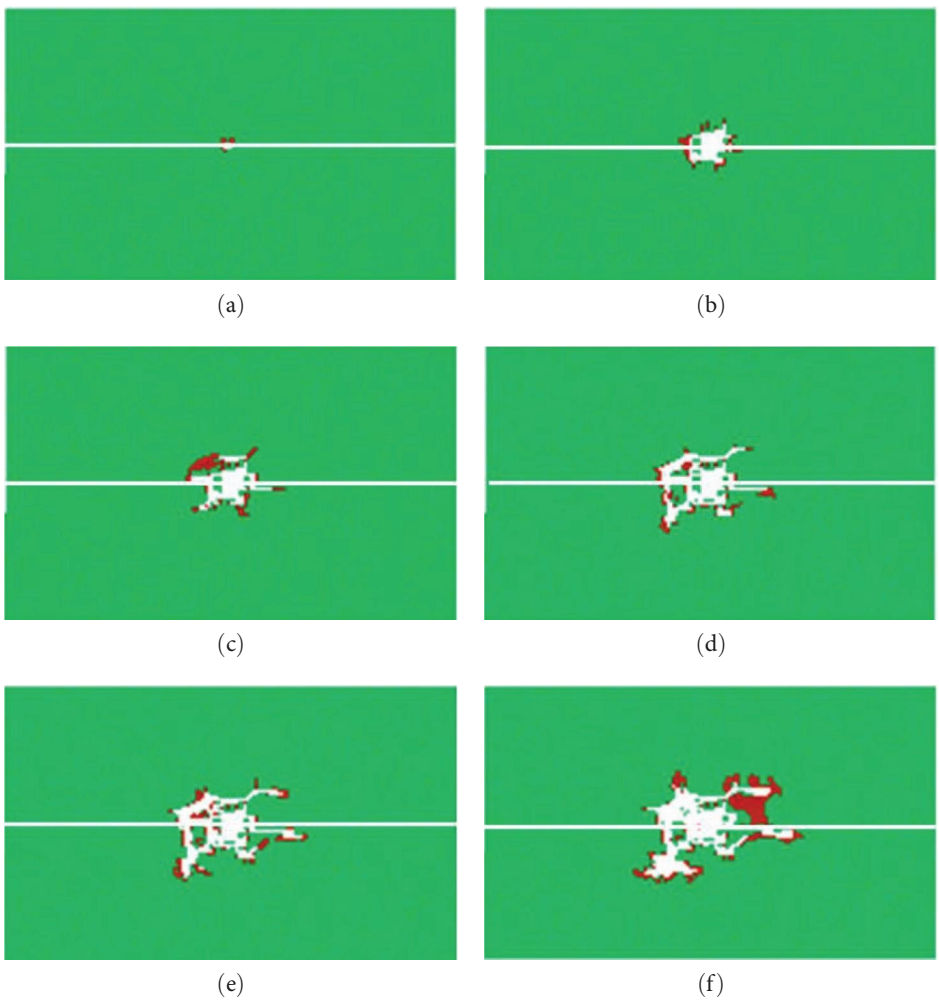

Figure 8: Characteristics of fracture growth during hydraulic fracturing: (a) Step 1, (b) Step 55, (c) Step 58, (d) Step 63, (e) Step 65, and (f) Step 68.

pressure is loaded under the influence of stress and water pressure, stress concentration takes place in the fracture section. With 6.6 MPa of water injection pressure in Step 48, there is a discernible concentration of water pressure. The coal seam is still intact at this point, and the impact of the pore water pressure is minimal. When water injection fracturing is increased to 8.6 MPa in Step 58, cracks start to appear and propagate in the direction of the maximum primary stress. As cracks emerge in the upward direction of the vertical seam thickness, pore water pressure relief occurs in the direction of seam thickness, showing the expansion of the pore water pressure's influence range. The fracture continues upward along the seam thickness direction to the coal–rock interface when fracturing is complete, and after deflection, it expands along the maximum primary stress direction. The influence range of pore water fracturing is roughly 80 m.

Numerous layers of broad fracture networks can be produced by hydraulic fracturing in deep boreholes along coal seams, according to studies. This implies that hydraulic fracturing-induced fractures may also grow vertically in

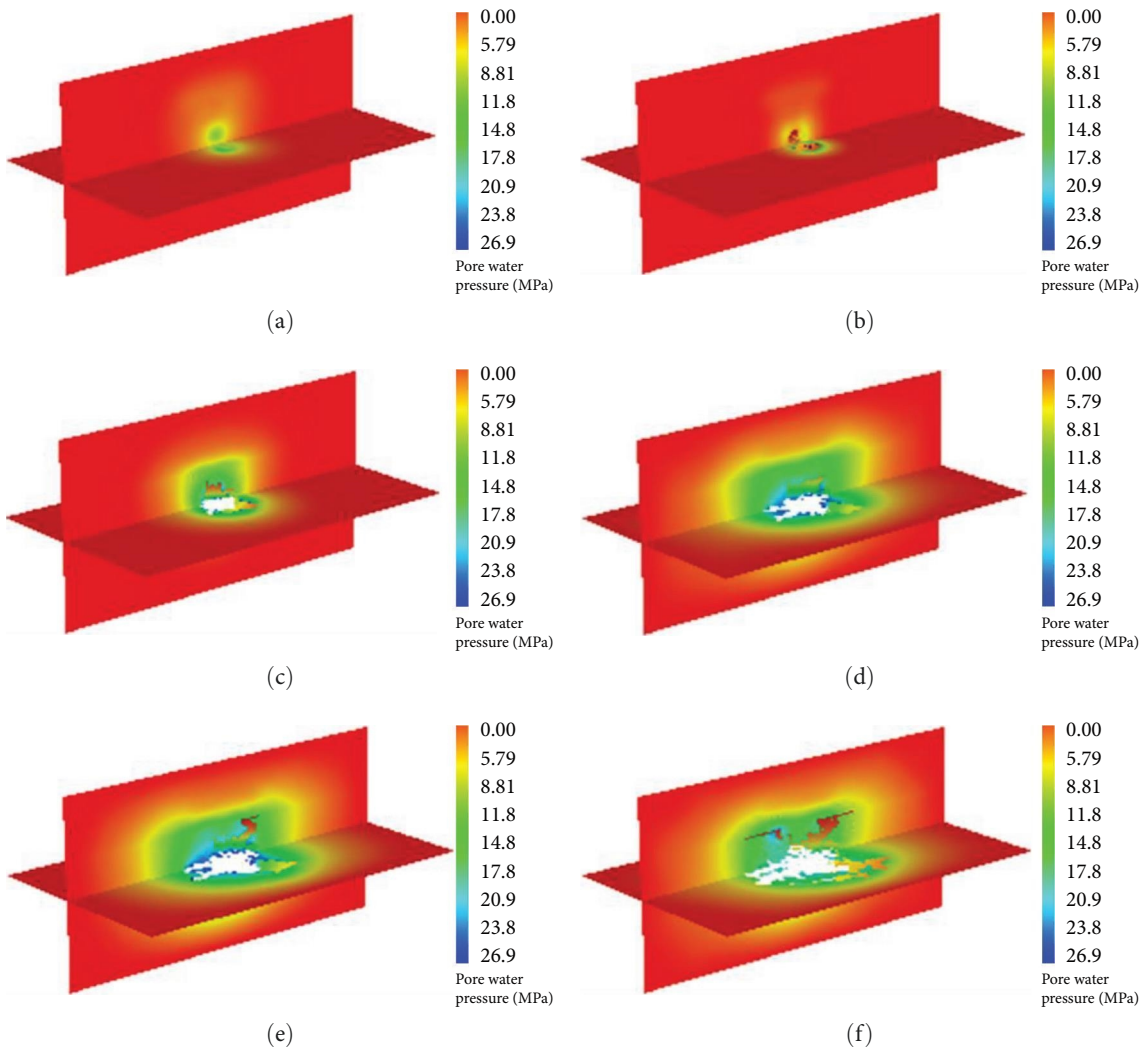

Figure 9: Cloud image of pore pressure during fracturing: (a) Step 1, (b) Step 48, (c) Step 58, (d) Step 63, (e) Step 65, and (f) Step 68.

addition to horizontally. Hydraulic fracturing can increase the volume of thick coal seams when seen in three dimensions.

4. Hydraulic Fracturing Drilling Construction Technology and Equipment

4.1. Hydraulic Fracturing Drilling Construction

4.1.1. Design Principles of Hydraulic Fracturing Boreholes. The drilling and fracturing process must be optimized to ensure efficient and effective operation based on the present state of hydraulic fracturing technology, coal mining equipment, and the geological features of the construction site.

(1) It is essential to take surface CBM extraction wells into account while developing the drilling layout. A minimum plane spacing of at least 40 m is required to prevent string holes.

(2) To ensure successful drilling and fracturing construction, it is crucial to steer clear of fault structures and minimize the impact of geological conditions.

(3) It is essential that the construction location is the actual coal deposit and that no previous boreholes have been dug to ensure successful drilling and fracturing.

(4) To ensure optimal results, it is imperative that the drilling design track meticulously follows the movement of each drill pipe in both vertical and horizontal directions without exceeding an angle of 0.6°. The smoothness of the drilling track is key to achieving this goal.

4.1.2. Drilling Process of Hydraulic Fracturing. The following describes the directional long-drilling hydraulic fracturing process:

(1) A drilling hydraulic fracturing design should be created based on the results of the drilling track and coal dust sample. Determining the fracturing procedure and the construction pressure, displacement, fracturing fluid volume, and other necessary elements should be included in this design.

(2) The precise positioning of the design, installation, and sampling drill for hydraulic fracturing tools at the designated location is absolutely crucial.
(3) Turn on the pump to start the fracturing process and pay particular attention to the injection pressure and flow curve. Before continuing, make sure the packer is firmly sealed.
(4) Once the packer seat is secured, the gear position and displacement are elevated to execute the fracturing process and achieve the intended injection volume of liquid.
(5) Move the tool string to the next fracturing stage for building when the pump has been stopped and the packer has been opened. Up until the point at which the fracturing process is finished, repeat Steps 1 through 4.

Before starting the pumping procedure for performing hydraulic fracturing, the operator on-site must control the injection pressure and perform a pressure test. The high-pressure valve at the port needs to be closed once the pressure gauge reaches the predetermined level in order to maintain that pressure. After stopping the pump, the pressure should not drop for at least 20 min. The pump pressure will significantly increase as the injection volume grows during the initial stage of the fracturing process. This will go on until the coal body fracture pressure threshold is reached by the fluid pressure in the hole. The coal body will crack at this moment, causing the injection pressure to peak before sharply dropping. To avoid unexpected pump stoppage and pressure decreases during the fracturing process, it is crucial to moderately manage the injection pressure. Field employees are required to keep meticulous records of the fracturing parameters, such as the water injection duration, pressure, and instantaneous flow rate. The gear must be adjusted in accordance with the circumstances in the hole while closely monitoring variations in pump injection pressure during fracturing. Operators should refrain from frequently shifting shifts that could cause unexpected pressure reductions or spikes.

4.2. Equipment Required for Drilling Yard Construction

4.2.1. Directional Drilling Rig. A completely hydraulic directional drilling rig known as ZDY6000LD (B) has been developed and constructed with success by the China Coal Science and Industry Group's Xi'an Research Institute Co., Ltd. It has been selected for deployment (as shown in Figure 10). The drilling machine possesses several advantages such as easy portability, wide range of speed adjustment, high torque, rational structure, advanced technical performance, strong process adaptability, effortless operation, and reliable safety. It is generally employed for the creation of highly precise directional drilling holes, such as those used for coal mine water injection, gas extraction, and geological exploration.

4.2.2. Directional Drill Pipe. The first is a Φ73 mm central cable drill pipe, as shown in Figure 11(a), which has the following characteristics:

Figure 10: ZDY6000LD (B) type drilling rig and pump truck.

(1) The drill pipe junction is joined to the drill pipe using friction welding and uses the internal thickening technique to locally enhance wall thickness. The drill pipe, which has an outer diameter of Φ73 mm, boasts great strength.
(2) The cable drill pipe and the YHD2-1000 (A) type MWD system can be utilized in conjunction during the drilling path measurement process to accurately assess the drilling parameters at the bottom of the borehole.
(3) The drill pipe has strong bending and torsion resistance, good rigidity, and a design strength that can withstand the demands of both hole bottom motor drilling and hole dynamic rotary drilling.

The second type is Φ73 mm nonmagnetic drill pipe made of nonmagnetic beryllium copper, as shown in Figure 11(b). To eliminate interference from regular steel drill pipe while measuring Azimuth angle and assure accurate measurement data, it is primarily used to position measuring instruments when drilling and measuring inclination. The three different types of nonmagnetic drill pipes are upper nonmagnetic drill pipe, outer probe pipe, and lower nonmagnetic drill pipe. The upper nonmagnetic drill pipe and the cable drill pipe share a central cable, and the outer probe pipe is used to install and fix the "probe pipe + probe tube battery cylinder.

4.2.3. Screw Motor. A screw motor with a curved angle was used to drill in one direction. A screw motor is a positive displacement energy converter that transforms liquid pressure energy into mechanical energy. By-pass valve assembly, screw motor (stator and rotor) assembly, universal shaft assembly, and driving shaft assembly make up the majority of its four pieces. Figure 12 shows a diagram of its construction.

There is no need to rotate the drill pipe when using a screw motor for near-horizontal directional drilling in a coal mine. Instead, the flushing liquid from the mud pump enters the motor through a bypass valve (or substitute joint), creating a pressure difference at the motor's entrance and exit that causes the motor rotor to rotate and transmit speed and torque to the drill through a universal shaft and drive shaft. By choosing or altering a different orienting tube by 0°−3°, different orienting effects can be obtained. The tool-facing angle of the outer pipe is changed by the data of inclination measurement while drilling, according to the intended drilling track, so that the inclination and orientation of the drilling can essentially approach the predetermined target.

(a) (b)

Figure 11: Hydraulic fracturing drill pipe: (a) Φ73 mm central cable drill pipe and (b) Φ73 mm nonmagnetic drill pipe.

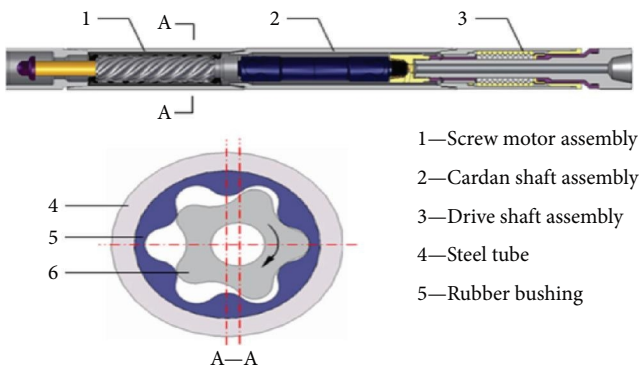

Figure 12: Schematic diagram of screw motor structure.

(a) (b)

Figure 13: Combined bit (PDC): (a) Φ94 mm tire PDC bit and (b) Φ193 mm reaming drill bit.

4.2.4. Directional Drill. Directional drilling two kinds of drill bits for drilling construction, respectively.

The first is a fetal PDC bit that measures 94 mm, as shown in Figure 13(a). The drill has a high wear resistance and is built of skeleton material and alloy that has been impregnated by sintering. Seven reinforced composite parts are welded into the flat-bottomed frame that serves as the drill's crown to provide it sufficient strength and longevity. To maintain the outer diameter of the bit body, polycrystals are placed around it. To ensure smooth water and slag discharge, a sizable aperture is placed in the center of the drill's top. The drill also has a significant capacity for breaking rock and can satisfy the demands of lengthy directional drilling in coal mines.

The second type is reaming drill bits (machining custom), which come in two sizes: Φ193 mm/153 mm (as indicated in Figure 13(b)) and Φ153 mm/113 mm. The hole device must be inserted while drilling in order to assist gas drainage when drilling. The Φ153 mm/113 mm reaming bit is mostly used for reaming drilling when opening holes.

4.2.5. In-Hole Fracturing Tool

(1) Packer. According to the drilling aperture and fracturing process, the packer was selected as a drag-type coal seam fracturing packer with a length of 1.62 m, a maximum outer diameter of 0.085 m, and a pass diameter of 0.05 m, as shown in Figure 14(a). The maximum pressure is 70 MPa, and the maximum temperature is 120°C.

(2) Differential Pressure Sleeve. According to Figure 14(b), the differential pressure slide sleeve has a length of 0.46 m, a maximum outer diameter of 0.085 m, and a pass diameter of 0.042 m. The maximum temperature is 120°C, and the maximum pressure is 70 MPa.

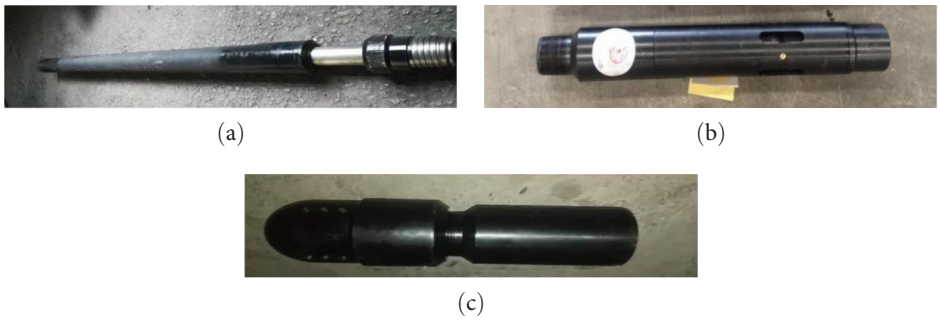

Figure 14: In-hole fracturing tool: (a) drag type coal seam fracturing packer, (b) differential pressure slide sleeve, and (c) single flow valve and guide shoe.

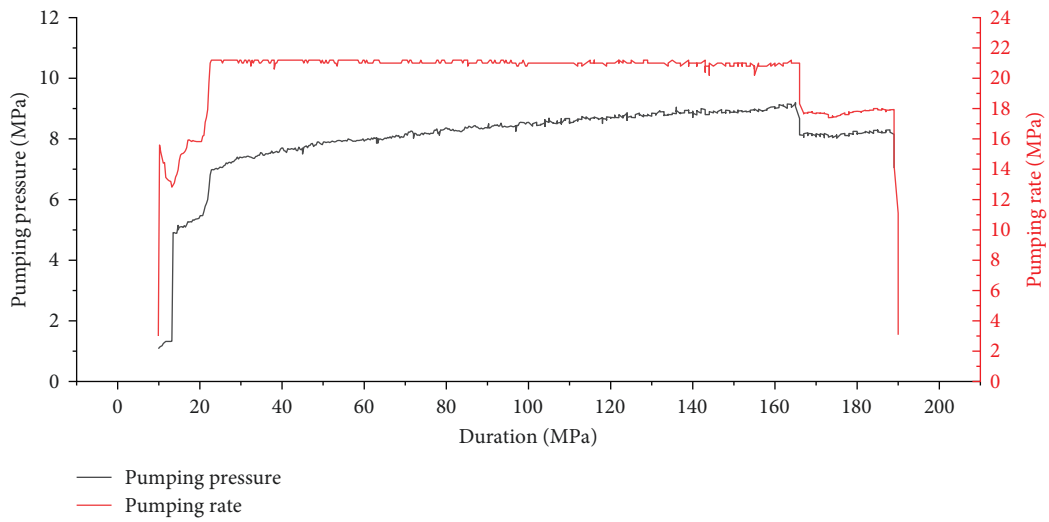

Figure 15: Typical fracturing curve.

(3) Single Flow Valve. The length of the single flow valve is 0.17 m, the maximum outer diameter is 0.085 m, and the pass diameter is 0.040 m, as shown in Figure 14(c).

According to Figure 14(c), the guiding shoe has a length of 0.18 m, a maximum outer diameter of 0. 085 m, and a maximum pressure of 70 MPa.

5. Investigation of Hydraulic Fracturing Effect

5.1. Fracturing Curve Analysis. As shown in Figure 15, during the first phase of fracturing, the pumping pressure for fracturing quickly surpasses the reservoir's extension pressure and begins to fracture coal, frequently concurrently with the biggest reservoir fracture extending cracks. The coal body's tightness coefficient (f) lies between 1.0 and 1.2. Because of the intricate geological formations and multiple faults in area 40103's working face, fractured area 4 has significantly developed macrocracks and separation systems, which lowers the coal body's compressive and tensile strengths.

A periodic "sawtooth" pattern can be seen on the pressure monitoring curve. Due to the combined filtration coefficient of the fracturing fluid, the hydraulic fracture fills and expands existing cracks as it advances during the rising stage of the curve to the anticipated depth of the coal seam. Complete communication between hydraulic and natural fractures takes place in the descending period of the curve, which causes a considerable rise in fracture volume and a subsequent loss of fracturing fluid by filtration. Minimal changes in maximum fracture extension pressure and minimum fracture closure pressure are seen during the intermediate stage of fracturing, indicating that pumping displacement is roughly equal to or close to the fluid loss from fractures into the coal seam within design parameters for fracture height. As anisotropic porous media with built-in pore cracks, coal seams only undergo the creation of fracture cracks when pore pressure exceeds fracture pressure thresholds. As a result, within the appropriate ranges and intervals, there are slight variations in the maximum fracture extension pressure as well as the minimum fracture closure pressure.

5.2. Transient Electromagnetic Monitoring. The newly created drilling transient electromagnetic detector by Xi'an Institute based on drilling push is meant to be employed, as shown in Figure 16(a). The excitation of the electromagnetic field and the data interaction and storage recording are completed in the drilling hole, and the three-component transient signal is measured.

The final hole distance, which is the geophysical exploration engineering design's maximum push distance, includes

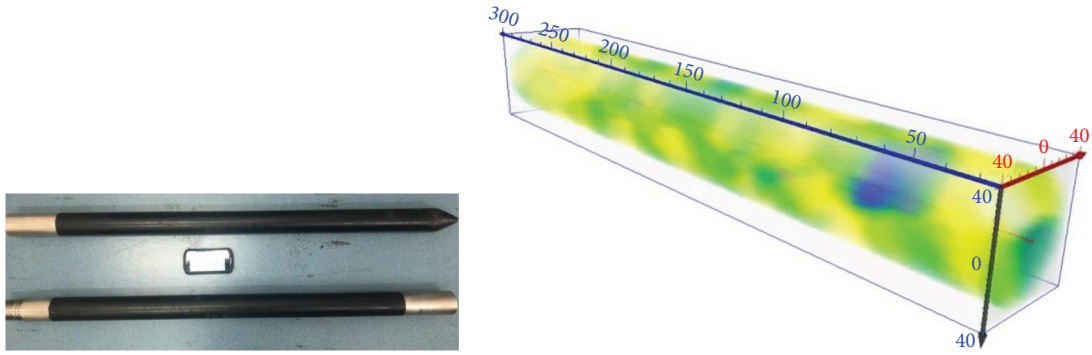

(a) (b)

Figure 16: Transient electromagnetic test equipment and results: (a) transient electromagnetic testing instruments and (b) results of transient electromagnetic probe fracturing radius.

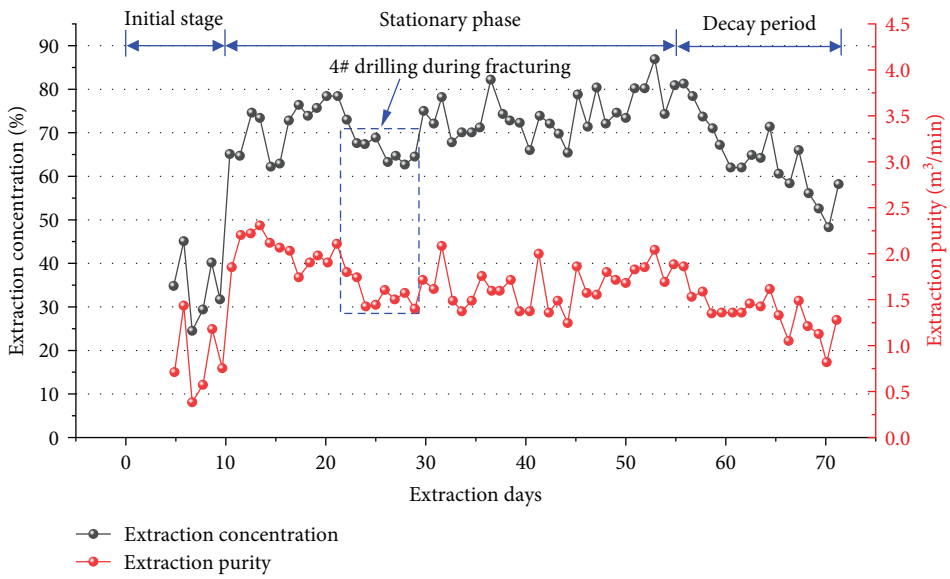

Figure 17: Gas extraction parameter curve of pressure hole.

a metal casing from 0 to 80 m in it that interferes strongly with transient electromagnetic detection. The drill pipe's length is 3 m during construction of the measuring point distance, and three components of data collection are performed at each measuring point. However, due to the actual construction project, the drilling rig pushed the geophysical instruments and drill pipe to more than 380 m, the drilling rig's pushing pressure display was abnormal, so the actual detection distance was 105−380 m inside the hole.

A thorough investigation determined the drilling and fracturing influence range to be between 38 and 46 m based on the findings of the transient electromagnetic test (Figure 16(b)). The extension and communication range of fracturing fractures can be determined based on changes in water flow by real-time monitoring of water seepage in the construction area during fracturing. For borehole 3#, the fracturing range is between 54 and 61 m, while for borehole 4, it is between 47 and 60 m.

5.3. Analysis of Gas Extraction Effect of Fracturing Borehole. In the 100-m borehole, the average extraction purity of gas was 0.320 m^3/min·hm during the monitoring period, and the average extraction concentration of pressure holes was 67.48%. In a 100-m well, the concentration of extracted gas is increased by 2.20–4.22 times compared to a conventional borehole, and the quantity of extracted pure gas is increased by 4.93–11.03 times. Figure 17 shows a comparison of pumping parameters.

Figure 17 illustrates the relationship between gas extraction concentration and purity of the fracturing borehole with extraction time. This relationship curve exhibits a general "rising-flattening-falling" trend, and its change process can be roughly divided into three stages: the initial extraction stage, the stable extraction stage, and the extraction decay stage. Because there is water in the fracturing borehole in the early stage of extraction and gas is difficult to flow under the impact of the water lock effect, the concentration and purity of gas are relatively lower than they are in the stable stage of extraction. The water lock effect decreases as pumping time increases, and the process moves into a steady pumping stage where the quantity and concentration of gas are higher. The

extraction decay period begins after a protracted period of extraction when the gas pressure and coal body's gas content start to decline.

The borehole's initial extraction stage has an average gas concentration of 40.38% and an average extraction purity of 1.23 m^3/min. The average extraction purity and gas concentration were 1.89 m^3/min and 73.01%, respectively. The typical gas concentration and extraction purity were, respectively, 63.63% and 1.51 m^3/min. In addition to causing existing cracks to widen and extend, high-pressure water can also cause main and secondary cracks to intertwine and constantly develop.

6. Conclusion

To meet the features of high ground stress and large gas emission in some coal seams, segmented hydraulic fracturing for gas extraction along directed long boreholes is proposed, using the Dafosi Mine as an example. Laboratory testing, numerical models, and field experiments were used to simulate crack expansion patterns and range by analyzing the coal seam's micropore structure. The following conclusions are reached:

(1) Coal seams' pore diameter, density, and connectedness can all be increased with hydraulic fracturing. The propagation of cracks during hydraulic fracturing in the 4# coal seam at Dafosi Mine was investigated using RFPA3D-flow numerical simulation software to examine the stress distribution around the crack under fluid-structure coupling and predict the radius of crack propagation.

(2) Directional long drilling in medium and hard coal seams along the coal seam was established using a segmented hydraulic fracturing technique. To find the best setting pressure levels, the stress and deformation properties of the rubber cylinder of the coal seam fracturing packer during setting and fracturing were examined. While perfecting hydraulic fracturing technology for long boreholes through strata of 4 coal seam at the Dafosi coal mine, advancements were made in construction and fracturing equipment.

(3) Open-hole drilling was investigated as a potential approach to examining the impacts of segmented hydraulic fracturing at the Dafosi mine. The influence radius of 46–58 m on coal seams after fracking was found by measuring the maximum fracture extension pressure and minimum fracture closure pressure during drilling and fracturing. Due to improved permeability properties from hydraulic fracturing, extraction concentration of gas increased by 2.20–4.22 times after fracking compared to pre-pumping boreholes without fracking and extraction volume increased by 4.93–11.03 times per 100 m.

Data Availability

All data generated or analyzed during this study are included in this published article.

Conflicts of Interest

The authors declare that they have no conflicts of interest.

Authors' Contributions

Chenyang Wang collected references, analyzed the measurement data, proposed the research method, and wrote this manuscript. Shugang Li, Li Liu, and Le Liu checked the method in review in this manuscript and verified its feasibility.

Acknowledgments

The authors acknowledge the financial support from the National Natural Science Foundation of China (5207042434) and the Shaanxi Provincial Natural Science Basic Research Program Project (2021JLM-26).

References

[1] Z. Sun, B. Huang, Y. Liu et al., "Gas-phase production equation for CBM reservoirs: interaction between hydraulic fracturing and coal orthotropic feature," *Journal of Petroleum Science and Engineering*, vol. 213, Article ID 110428, 2022.

[2] X. Wang, Q. Hu, and Q. Li, "Investigation of the stress evolution under the effect of hydraulic fracturing in the application of coalbed methane recovery," *Fuel*, vol. 300, no. 3, Article ID 120930, 2021.

[3] Y. Fan, L. Shu, Z. Huo, J. Hao, and Y. Li, "Numerical simulation research on hydraulic fracturing promoting coalbed methane extraction," *Shock and Vibration*, vol. 2021, Article ID 3269592, 12 pages, 2021.

[4] L. Si, Z. Li, M. Kizil, Z. Chen, Y. Yang, and S. Ji, "The influence of closed pores on the gas transport and its application in coal mine gas extraction," *Fuel*, vol. 254, Article ID 115605, 2019.

[5] L. Wang, Z. Lu, D.-P. Chen et al., "Safe strategy for coal and gas outburst prevention in deep-and-thick coal seams using a soft rock protective layer mining," *Safety Science*, vol. 129, no. 1, Article ID 104800, 2020.

[6] E. Zhao, K. Li, X. Yang, and N. Deng, "Speculum observation and trajectory measurement in gas extraction drilling: a case study of Changling coal mine," *Geofluids*, vol. 2021, Article ID 5545067, 16 pages, 2021.

[7] W. Liang, J. Yan, B. Zhang, and D. Hou, "Review on coal bed methane recovery theory and technology: recent progress and perspectives," *Energy & Fuels*, vol. 35, no. 6, pp. 4633–4643, 2021.

[8] B. Shi, Y. Cao, L. Tian, J. Zhang, and S. Liu, "CO_2 gas fracturing in high dip angled coal seams for improved gas drainage efficiency at Hashatu coal mine," *Energy & Fuels*, vol. 36, no. 5, pp. 2763–2774, 2022.

[9] J. Liu, Y. Qin, T. Zhou, and Y. Gao, "Dual-porosity coupled borehole gas flow model: a new method for inversion of coal seam permeability," *Natural Resources Research*, vol. 29, pp. 3957–3971, 2020.

[10] H. Cheng, N. Zhang, Y. Yang, W. Peng, and H. Chen, "A study on the mechanical mechanism of injection heat to increase production of gas in low-permeability coal seam," *Energies*, vol. 12, no. 12, Article ID 2332, 2019.

[11] Z. Zhang, E. Wang, H. Zhang, Z. Bai, Y. Zhang, and X. Chen, "Research on nonlinear variation of elastic wave velocity dispersion characteristic in limestone dynamic fracture process,"

Fractals—an Interdisciplinary Journal on the Complex Geometry of Nature, vol. 31, no. 1, Article ID 2350008, 2023.

[12] L. Li and W. Wu, "Variation law of roof stress and permeability enhancement effect of repeated hydraulic fracturing in low-permeability coal seam," *Energy Science & Engineering*, vol. 9, no. 9, pp. 1501–1516, 2021.

[13] L. Chen, Z. Ge, B. Xia et al., "Research on hydraulic technology for seam permeability enhancement in underground coal mines in China," *Energies*, vol. 11, no. 2, Article ID 427, 2018.

[14] B. Jiang, S. Gu, W. Li, G. Zhang, and J. Zhang, "Case studies of comprehensive gas control method during fully mechanized caving of low-permeability ultrathick coal seams," *Geofluids*, vol. 2021, Article ID 5558678, 14 pages, 2021.

[15] Y. Cao, J. Zhang, H. Zhai, G. Fu, T. Lin, and S. Liu, "CO_2 gas fracturing: a novel reservoir stimulation technology in low permeability gassy coal seams," *Fuel*, vol. 203, pp. 197–207, 2017.

[16] Y. Fan, B. Qin, Q. Zhou, Q. Shi, D. Ma, and J. Wu, "Liquid CO_2 phase transition fracturing technology and its application in enhancing gas drainage of coal mines," *Adsorption Science and Technology*, vol. 38, no. 9-10, pp. 393–412, 2020.

[17] K. Y. Cao, S. H. Son, J. Moon, and J. S.-I. Kwon, "A closed-loop integration of scheduling and control for hydraulic fracturing using offset-free model predictive control," *Applied Energy*, vol. 302, Article ID 117487, 2021.

[18] W. A. M. Wanniarachchi, P. G. Ranjith, M. S. A. Perera, T. D. Rathnaweera, D. C. Zhang, and C. Zhang, "Investigation of effects of fracturing fluid on hydraulic fracturing and fracture permeability of reservoir rocks: an experimental study using water and foam fracturing," *Engineering Fracture Mechanics*, vol. 194, pp. 117–135, 2018.

[19] J. Zhang, L. Si, J. Chen, M. Kizil, C. Wang, and Z. Chen, "Stimulation techniques of coalbed methane reservoirs," *Geofluids*, vol. 2020, Article ID 5152646, 23 pages, 2020.

[20] S. Chen, J. Zhang, D. Yin, F. Li, J. Lu, and P. Zhu, "Visualizing experimental investigation on gas—liquid replacements in a microcleat model using the reconstruction method," *Deep Underground Science and Engineering*, vol. 2, no. 3, pp. 295–303, 2023.

[21] W. Wang, S. Lu, M. Li, and C. Wang, "Coal breakage impact by high-pressure water jet and induced pressure relief and permeability enhancement by hydraulic flushing cavity: mechanism and application," *Arabian Journal of Geosciences*, vol. 14, Article ID 2399, 2021.

[22] Y. Song, W. Lu, C. He, and E. Bai, "Numerical simulation of the influence of natural fractures on hydraulic fracture propagation," *Geofluids*, vol. 2020, Article ID 8878548, 12 pages, 2020.

[23] S. Nainar and S. K. Govindarajan, "Semi-analytic analysis and optimization of stress-dependent permeability model for the coal bed methane gas reservoir," *Environmental Earth Sciences*, vol. 80, no. 7, Article ID 272, 2021.

[24] P. Mou, J. Pan, K. Wang, J. Wei, Y. Yang, and X. Wang, "Influences of hydraulic fracturing on microfractures of high-rank coal under different in-situ stress conditions," *Fuel*, vol. 287, Article ID 119566, 2021.

[25] Y. Lu, L. Wang, Z. Ge, Z. Zhou, K. Deng, and S. Zuo, "Fracture and pore structure dynamic evolution of coals during hydraulic fracturing," *Fuel*, vol. 259, Article ID 116272, 2020.

[26] Z. Liu, A. Cao, X. Guo, and J. Li, "Deep-hole water injection technology of strong impact tendency coal seam—a case study in Tangkou coal mine," *Arabian Journal of Geosciences*, vol. 11, no. 2, Article ID 12, 2018.

[27] X. Li, D. Chen, J. Fu, S. Liu, and X. Geng, "Construction and application of fuzzy comprehensive evaluation model for rockburst based on microseismic monitoring," *Applied Science*, vol. 13, no. 21, Article ID 12013, 2023.

[28] X. Chen, W. Shan, R. Sun, and L. Zhang, "Methane displacement characteristic of coal and its pore change in water injection," *Energy Exploration & Exploitation*, vol. 38, no. 5, pp. 1647–1663, 2020.

[29] J. Zhao and D. Guo, "Cracking mechanism of coal under high-pressure water jet and its applications for enhanced coalbed methane drainage," *Arabian Journal of Geosciences*, vol. 11, Article ID 427, 2018.

[30] D. Yin, S. Chen, Y. Ge, and R. Liu, "Mechanical properties of rock–coal bi-material samples with different lithologies under uniaxial loading," *Journal of Materials Research and Technology*, vol. 10, no. 1, pp. 322–338, 2021.

[31] H. Li, X. Li, J. Fu et al., "Experimental study on compressive behavior and failure characteristics of imitation steel fiber concrete under uniaxial load," *Construction and Building Materials*, vol. 399, no. 8, Article ID 132599, 2023.

[32] S. Song, S. Wang, S. Jiang, Y. Liang, and P. Hu, "Multifield coupled dynamic simulation of coal oxidation and self-heating in longwall coal mine gob," *Mathematical Problems in Engineering*, vol. 2020, Article ID 9075657, 16 pages, 2020.

[33] M. Zhai, D. Wang, Z. Zhang et al., "Numerical simulation and multi-factor optimization of hydraulic fracturing in deep naturally fractured sandstones based on response surface method," *Engineering Fracture Mechanics*, vol. 259, Article ID 108110, 2022.

[34] L. Rybarska-Rusinek, E. Rejwer, and A. Linkov, "Speeded simulation of seismicity accompanying mining and hydro-fracture," *Engineering Computations*, vol. 35, no. 5, pp. 1932–1949, 2018.

[35] Z. Zhang, E. Wang, N. Li, H. Zhang, Z. Bai, and Y. Zhang, "Research on macroscopic mechanical properties and microscopic evolution characteristic of sandstone in thermal environment," *Construction and Building Materials*, vol. 366, Article ID 130152, 2023.

[36] H. Liu, X. Li, Z. Yu et al., "Influence of hole diameter on mechanical properties and stability of granite rock surrounding tunnels," *Physics of Fluids*, vol. 35, no. 6, Article ID 064121, 2023.

[37] J. Zou, W. Chen, D. Yang, J. Yuan, and Y.-Y. Jiao, "Fractal characteristics of the anisotropic microstructure and pore distribution of low-rank coal," *AAPG Bulletin*, vol. 103, no. 6, pp. 1297–1319, 2019.

[38] J. Fu, D. Chen, X. Li et al., "Research on the technology of gob-side entry retaining by pouring support beside the roadway in "three soft" coal seam: a case study," *Physics of Fluids*, vol. 36, Article ID 017123, 2024.

[39] M. Cheng, X. Fu, and J. Kang, "Compressibility of different pore and fracture structures and its relationship with heterogeneity and minerals in low-rank coal reservoirs: an experimental study based on nuclear magnetic resonance and micro-CT," *Energy & Fuels*, vol. 34, no. 9, pp. 10894–10903, 2020.

[40] H. Li, X. Li, J. Fu, Z. Gao, P. Chen, and Z. Zhang, "Research on acoustic emission multi-parameter characteristics in the failure process of imitation steel fiber reinforced concrete," *Physics of Fluids*, vol. 35, Article ID 107109, 2023.

[41] W. Lu, B. Huang, and X. Zhao, "A review of recent research and development of the effect of hydraulic fracturing on gas

adsorption and desorption in coal seams," *Adsorption Science & Technology*, vol. 37, no. 5-6, pp. 509–529, 2019.

[42] J. Li, Q. Huang, G. Wang, E. Wang, S. Ju, and C. Qin, "Experimental study of effect of slickwater fracturing on coal pore structure and methane adsorption," *Energy*, vol. 239, Article ID 122421, 2022.

[43] J. Xie, J. Xie, G. Ni, S. Rahman, S. Qian, and W. Hui, "Effects of pulse wave on the variation of coal pore structure in pulsating hydraulic fracturing process of coal seam," *Fuel*, vol. 264, Article ID 116906, 2020.

[44] M.-M. Kou, X.-R. Liu, Z.-Q. Wang, and S.-D. Tang, "Laboratory investigations on failure, energy and permeability evolution of fissured rock-like materials under seepage pressures," *Engineering Fracture Mechanics*, vol. 247, no. 1–4, Article ID 107694, 2021.

[45] X.-Y. Sun, C.-H. Ho, C. Li, Y. Xia, and Q. Zhang, "Inclination effect of coal mine strata on the stability of loess land slope under the condition of underground mining," *Natural Hazards*, vol. 104, no. 1, pp. 833–852, 2020.

[46] P. Wang, L.-S. Jiang, P.-Q. Zheng, G.-P. Qin, and C. Zhang, "Inducing mode analysis of rock burst in fault-affected zone with a hard–thick stratum occurrence," *Environmental Earth Sciences*, vol. 78, no. 15, pp. 467 1–467 13, 2019.

[47] F. Xiao, M. Xin, L. Li et al., "Thermos-solid-gas coupling dynamic model and numerical simulation of coal containing gas," *Geofluids*, vol. 2020, Article ID 8837425, 9 pages, 2020.

[48] Y. Zhao, Y. Zhang, H. Yang, Q. Liu, and G. Tian, "Experimental study on relationship between fracture propagation and pumping parameters under constant pressure injection conditions," *Fuel*, vol. 307, Article ID 121789, 2022.

[49] K. Duan, C. Y. Kwok, W. Wu, and L. Jing, "DEM modeling of hydraulic fracturing in permeable rock: influence of viscosity, injection rate and in situ states," *Acta Geotechnica*, vol. 13, no. 5, pp. 1187–1202, 2018.